Trajectory Studies of Methyl Radical Reaction with Iodine Molecule

Sang Kwon Lee, Jongbaik Ree, Yoo Hang Kim,†,* and Hyung Kyu Shin‡

Department of Chemistry Education and Institute of Science Education, Chonnam National University, Gwangju 500-757, Korea
†Department of Chemistry and Center for Chemical Dynamics, Inha University, Incheon 402-751, Korea
**E-mail: yhkim@inha.ac.kr*
‡Department of Chemistry, University of Nevada, Reno, Nevada 89557, U. S. A.
Received March 19, 2005

The reaction of methyl radical with iodine molecule on an attractive potential energy surface is studied by classical trajectory procedures. The reaction occurs over a wide range of impact parameters with the majority of reactive events occurring in the backward rebound region on a subpicosecond scale. A small fraction of reactive events take place in the forward hemisphere on a longer time scale. The ensemble average of reaction times is 0.36 ps. The occurrence of reactive events is strongly favored when the incident radical and the target molecule align in the neighborhood of collinear geometry. Since the rotational velocity of I_2 is slow, the preferential occurrence of reactive events at the collinear configuration of $CH_3 \cdots I \cdots I$ leads to the reaction exhibiting an anisotropic dependence on the orientation of I_2. During the collision, there is a rapid flow of energy from the $H_3C \cdots I$ interaction to the I-I bond. The CH_3I translation and H_3C-I vibration share nearly all the energy released in the reaction, and the distribution of the vibrational energy is statistical. The reaction probability is $\cong 0.4$ at the CH_3 and I_2 temperatures maintained at 1000 K and 300 K, respectively. The probability is weakly dependent on the CH_3 and I_2 temperatures between 300 K and 1500 K.

Key Words : Classical trajectory, Methyl radical, Iodine

Introduction

The methyl radical is a highly reactive intermediate in many combustion processes involving hydrocarbon,[1-3] and its reactions with halogen molecules are known to be important in the photohalogenation of hydrocarbons and in the photolysis and pyrolysis of alkyl halides.[4-10] The reaction dynamics of methyl radicals interacting with halogen or interhalogen molecules have received considerable attention.[4,11-15] In particular the reaction of methyl radicals with heavy iodine molecules $CH_3+I_2 \rightarrow CH_3I+I$ is a prototypical model system for polyatomic species reacting on a strongly attractive potential energy surface and is an ideal system for which trajectory procedures can be applied.

An advantage of such procedures is that an intuitive insight into the dynamics is gained, since we can follow a reaction path starting from an initial state especially during the course of reactive interaction and product formation, gaining valuable information on dynamical aspects of energy transfer, bond dissociation and bond formation.[16-18] This reaction, which proceeds through a low energy barrier, is dominated by a short-range interaction and is representative of short-time reaction dynamics. Thus, studies of this type of reaction can provide valuable information for the development of a comprehensive approach to the reaction dynamics of atoms and free radicals with various molecules including polyatoms. In a recent paper, we have shown that this exothermic reaction takes place on a short-time scale (< 1 ps) in a "direct mode" collision.[13] Zewail and his asssociates have studied direct clocking of the CH_3I dissociation in the reverse process, showing the dynamics of the CH_3-I bond dissociation and the inelastic process of CH_3I+I on a femtosecond scale.[12] Earlier studies show that the rate of H atom abstraction reaction is enhanced by hot methyl radicals.[19-23] Kovalenko and Leone have observed such enhancement in the reactions of CH_3 with Cl_2 and Br_2 when hot methyl radicals produced in the dissociation of CH_3I are used.[4] Their studies show that the enhancement is due largely to the translational excitation.

During a bimolecular encounter, a transient species can form, and the intramolecular process of energy transfer from one part of this species to another is a prerequisite to the occurrence of subsequent bond dissociation steps. Therefore, the nature of intramolecular energy flow and the length of the time scale of such processes during the course of interaction primarily determine the outcome of a chemical reaction. In this work we use classical dynamics procedures to study the distributions of reaction times including long-time events, orientation dependence of reactive events, and product vibrational and translational excitation in $CH_3 + I_2 \rightarrow CH_3I + I$. For this purpose, we solve the equations of motion for the reaction system on a potential energy surface over a wide range of impact parameters at Maxwellian collisional energies using the procedures outlined in Ref. 13.

Interaction Model

Rigorous treatment of the reaction requires knowledge of the interaction potential at all atom-atom distances throughout the course of reaction, and the formulation of such potential function for a six-atom collision system requires tremendous computational efforts. Although it is not feasible

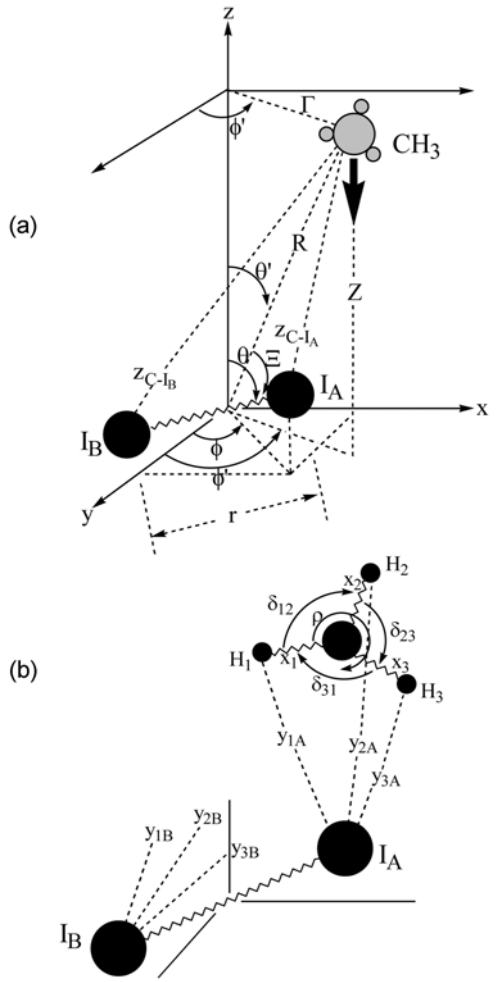

Figure 1. (a) Model for the collision of CH_3 with I_2, showing the interatomic coordinates and rotational angles. For convenience, the iodine atoms are denoted by I_A and I_B. The position of C is defined by (Z, Γ, ϕ') and I_2 is defined by (r, θ, ϕ). (b) Details of the interatomic distances are displayed. To define the interatomic coordinates, the three hydrogen atoms are identified as H_1, H_2 and H_3.

to set up a quantitatively accurate potential energy surface for the reaction between CH_3 and I_2, any physically realistic potential must include all important atom-atom interactions which are coupled with the reaction coordinate. To set up such a potential, we choose a cylindrical coordinate system such that the direction of the relative velocity vector coincides with the z axis and the origin is at the center of mass of I_2 (see Figure 1)[13,24,25] The reaction can occur through either the C to I_A or C to I_B interaction, in which the interatomic distance is

$$z_{CI_A,I_B} = \left[R^2 \pm \frac{1}{4}r^2 - rR\cos\Xi\right]^{1/2},$$

where R is the distance between the centers of mass of the collision system, which is $(Z^2+\Gamma^2)^{1/2}$, where Γ is the distance between C and the z axis. Note that the initial $(t \to -\infty)$ value of Γ is the impact parameter b. Here r is the I-I bond distance, and the orientation angle Ξ between the I_2 molecular axis and R is $\cos\Xi = \cos\theta\cos\theta' + \sin\theta\sin\theta'\cos(\phi-\phi')$.

While these C to I interactions are the primary driver for the production of CH_3I, the three hydrogen atoms can contribute significantly to the motion of the CH_3 radical along the $H_3C\cdots I\cdots I$ reaction coordinate. Unlike the photodissociation of CH_3I, where the reaction starts out with the stable CH_3I configuration and the fragments recoil through the mechanics of the "half-collision",[26,27] the present collision-initiated reactive process involves the participation of H atoms over the full range of interaction. When CH_3 approaches the iodine atoms, these hydrogen atoms undergo nonbonding interactions with the I atoms, thus steering the carbon atom toward the reaction coordinate and then steering CH_3-I away from the fragment I. Thus, it will be necessary to represent each H to I interaction energy which becomes sufficiently repulsive so that the H atom does not approach too close to the iodine atoms. This type of interaction will then ensure the non-occurrence of reaction between H and I. Furthermore, CH_3 undergoes the rotation around the C_3 axis, the C-H stretching vibrations, and the H-C-H bending vibrations, all of which will affect the position of each H atom from I_A or I_B at any instant during the collision. Therefore, the overall interaction energy includes, in addition to the C-I_A and C-I_B interactions, the six H_i to I interactions, where i = 1, 2, 3, the three C-H_i stretches, and the three H_i-C-H_j bends (ij = 12, 23, 31). We denote the interatomic distances for H_i-I_A and H_i-I_B by y_{iA} and y_{iB}, the H_i-C bond vibrational displacements by x_i, and the H_i-C-H_j angle by δ_{ij}. Thus, the complete coordinate system is (r, θ, ϕ, Z, Γ, ϕ', {y_A}, {y_B}, {x}, {δ}, ρ), where {y_A} ≡ {y_{1A}, y_{2A}, y_{3A}}, {y_B} ≡ {y_{1B}, y_{2B}, y_{3B}}, {x} ≡ {x_1, x_2, x_3}, {δ} ≡ {δ_{12}, δ_{23}, δ_{31}}, and ρ is the rotation of CH_3 around the C_3 axis. Note that for the simple C+I_2 collision, the coordinate system would be (r, θ, ϕ, Z, Γ, ϕ'). By rotating the coordinate system about the z axis, we can eliminate the azimuthal angle ϕ' from the relative system, *i.e.*, $\Xi = \Xi(r, \theta, \phi, Z, \Gamma)$. We thus use the coordinate system (r, θ, ϕ, Z, Γ, {y_A}, {y_B}, {x}, {δ}, ρ). Here, the H_1 to I_A and H_1 to I_B distances are, respectively,

$$y_{1A} = \{R_1^2 + (d_{CH}+x_1)^2 + 2R_1(d_{CH}+x_1)\sin(\chi\cos\rho_1)\}^{1/2} \quad (1a)$$

$$y_{1B} = \{R_2^2 + (d_{CH}+x_1)^2 + 2R_2(d_{CH}+x_1)\sin(\eta\cos\rho_1)\}^{1/2} \quad (1b)$$

where,

$$R_1 = \left\{R^2 + \frac{r^2}{4} - rR\cos\Xi\right\},$$

$$R_2 = \left\{R^2 + \frac{r^2}{4} + rR\cos\Xi\right\},$$

$$\sin\chi = \frac{r}{2R_1}\sin\Xi,$$

$$\sin\eta = \frac{r}{2R_2}\sin\Xi.$$

Four other distances y_{2A}, y_{2B}, y_{3A}, y_{3B} can be obtained similarly.

The interaction potential energy constructed in terms of the reaction coordinates C-I_A, C-I_B and I_A-I_B becomes modified by the interaction energies representing the six H-I interactions, the three H-C stretches, and the three H-C-H bends. We express the potential energies corresponding to these motions by

$$V_{H_i-I_A}(y_{iA}) = D_{HI}e^{\alpha - y_{iA}/a_{HI}},\ i = 1, 2, 3 \tag{2a}$$

$$V_{H_i-I_B}(y_{iB}) = D_{HI}e^{\alpha - y_{iB}/a_{HI}},\ i = 1, 2, 3 \tag{2b}$$

$$V_{C\text{-}H_i}(x_i) = D_{CH}[e^{(x_e - x_i)a_{CH}} - 2e^{(x_e - x_i)2a_{CH}}],\ i = 1, 2, 3 \tag{2c}$$

$$V_{H_i-C-H_j}(\delta_{ij}) = \frac{1}{2}k_\delta\delta_{ij}^2,\ ij = 12, 23, 31 \tag{2d}$$

The first two functions have a complicated dependence on r, θ, ϕ, Z, Γ, x_i, δ_{ij}, and ρ as shown in Eq. (1). D_{HI} determines the strength of the H-I interaction, α is a positive potential parameter which can be adjusted to make the interaction sufficiently repulsive such that the hydrogen atoms do not approach too close to the iodine atoms, and a_{HI} is an exponential range parameter. In these two equations, the potential parameters can be combined as $D_{HI}' = D_{HI}e^{\alpha}$, but we use the above form since it conforms to the usual form of exponential potential functions and is convenient for choosing physically reasonable values of the energy and distance parameters (D_{HI}, α). Equation (2c) is the Morse form designed to describe the C-H stretching motion with the usual potential parameters D_{CH} and a_{CH}. In Eq. (2d), K_δ is the force constant of the H-C-H bending motion. Throughout this paper, the subscript "e" represents the equilibrium value of the distance indicated.

The strategy in setting up the overall potential energy is first to formulate the principal skeletal interaction described by (r, θ, ϕ, Z, Γ) for the C-I_A and C-I_B interaction in the London-Eyring-Polanyi-Sato form,[28] and then to modify it with the H-I interactions, C-H vibrations and H-C-H bends, which introduce the additional coordinates ($\{y_A\}$, $\{y_B\}$, $\{x\}$, $\{\delta\}$, ρ) in the potential energy, modifying the topology of the reaction-zone PES significantly. Thus, the final form of the PES, which now includes the subtle features coming from the presence of the three hydrogen atoms, is dependent on (r, θ, ϕ, Z, Γ, $\{y_A\}$,$\{y_B\}$,$\{x\}$,$\{\delta\}$, ρ). The overall potential energy can then be constructed in the modified LEPS version as

$$\begin{aligned} U = Q_{II} &+ \left(Q_{CI_A} + \sum_{i=1}^{3} D_{HI}e^{\alpha - y_{iA}/a_{HI}}\right) + \left(Q_{CI_B} + \sum_{i=1}^{3} D_{HI}e^{\alpha - y_{iB}/a_{HI}}\right) \\ &- \left\{A_{II}^2 + \left(A_{CI_A} + \sum_{i=1}^{3} D_{HI}e^{\alpha - y_{iA}/a_{HI}}\right)^2 + \left(A_{CI_B} + \sum_{i=1}^{3} D_{HI}e^{\alpha - y_{iB}/a_{HI}}\right)^2\right. \\ &- A_{II}\left[\left(A_{CI_A} + \sum_{i=1}^{3} D_{HI}e^{\alpha - y_{iA}/a_{HI}}\right) + \left(A_{CI_B} + \sum_{i=1}^{3} D_{HI}e^{\alpha - y_{iB}/a_{HI}}\right)\right] \\ &\left. - \left(A_{CI_A} + \sum_{i=1}^{3} D_{HI}e^{\alpha - y_{iA}/a_{HI}}\right)\left(A_{CI_B} + \sum_{i=1}^{3} D_{HI}e^{\alpha - y_{iB}/a_{HI}}\right)\right\}^{\frac{1}{2}} \\ &+ \frac{1}{2}\sum_{i\neq j} k_\delta\delta_{ij}^2 + \sum_{i=1}^{3} D_{CH}[e^{(x_e - x_i)/a_{CH}} + 2e^{(x_e - x_i)/2a_{CH}}], \end{aligned} \tag{3}$$

where the Coulomb and exchange terms for the I to I, C to I_A, and C to I_B interactions are

$$\begin{aligned} Q_{II} &= \frac{1}{4}[D_{II}/(1 + \Delta_{II})] \\ &\times [(3 + \Delta_{II})e^{(r_e - r)/a_{II}} - (2 + 6\Delta_{II})e^{(r_e - r)/2a_{II}}] \end{aligned} \tag{4a}$$

$$\begin{aligned} A_{II} &= \frac{1}{4}[D_{II}/(1 + \Delta_{II})] \\ &\times [(1 + 3\Delta_{II})e^{(r_e - r)/a_{II}} - (6 + 2\Delta_{II})e^{(r_e - r)/2a_{II}}], \end{aligned} \tag{4b}$$

$$\begin{aligned} Q_{CI_A} &= \frac{1}{4}[D_{CI_A}/(1 + \Delta_{CI_A})][(3 + \Delta_{CI_A})e^{(z_{e,CI_A} - z_{CI_A})/a_{CI_A}} \\ &- (2 + 6\Delta_{CI_A})e^{(z_{e,CI_A} - z_{CI_A})/2a_{CI_A}}], \end{aligned} \tag{4c}$$

$$\begin{aligned} A_{CI_A} &= \frac{1}{4}[D_{CI_A}/(1 + \Delta_{CI_A})][(1 + 3\Delta_{CI_A})e^{(z_{e,CI_A} - z_{CI_A})/a_{CI_A}} \\ &- (6 + 2\Delta_{CI_A})e^{(z_{e,CI_A} - z_{CI_A})/2a_{CI_A}}], \end{aligned} \tag{4d}$$

$$\begin{aligned} Q_{CI_B} &= \frac{1}{4}[D_{CI_B}/(1 + \Delta_{CI_B})][(3 + \Delta_{CI_B})e^{(z_{e,CI_B} - z_{CI_B})/a_{CI_B}} \\ &- (2 + 6\Delta_{CI_B})e^{(z_{e,CI_B} - z_{CI_B})/2a_{CI_B}}], \end{aligned} \tag{4e}$$

$$\begin{aligned} A_{CI_B} &= \frac{1}{4}[D_{CI_B}/(1 + \Delta_{CI_B})][(1 + 3\Delta_{CI_B})e^{(z_{e,CI_B} - z_{CI_B})/a_{CI_B}} \\ &- (6 + 2\Delta_{CI_B})e^{(z_{e,CI_B} - z_{CI_B})/2a_{CI_B}}], \end{aligned} \tag{4f}$$

respectively, where Δ_i's are the adjustable Sato parameters which allow a variety of experimental situations, especially the magnitude of the barrier height, to be modeled. We have grouped the three H-I_A interactions with C-I_A for the CH_3-I_A interaction and H-I_B interactions with C-I_B for the CH_3-I_B

Table 1. Interaction parameters

Interaction	i = I-I	C-I	C-H
D_i (eV)†	1.556[29]#	2.363[30]	4.953[30]**
ω_i (cm^{-1})	214.5[29]	533.2[30]	3228[31]
$r_{e,i}$ (Å)	2.666[29]	2.139[30]	1.079[30]
a_i (Å)*	0.269	0.290	0.264

For the H to I interaction, the best-fit values are D_{HI} = 0.0015 eV, a_{HI} = 0.4 Å, and α = 6.85.

For the H-C-H bending, using the procedure given in Herzberg's book[32] and $k_1 = 5.950 \times 10^2$ Newton/m,[33] we find $k / \lambda^2 = 3.483 \times 10$ Newton/m and $\mu_\delta = 5.032 \times 10^{-28}$ kg.

For the CH_3 rotation, the rotational constant is 9.57 cm^{-1}.[30]

†$D_i = D_{0,i}^0 + \frac{1}{2}\hbar\omega_i$, where $D_{0,i}^0$ is taken from the references.

#Parentheses include references.

*Calculated from $a_i = (D_i/2\mu_i)^{1/2}/\omega_i$.

interaction in Eq. (3). Here D is the depth of the potential well and a is the range parameter of the exponential interaction indicated. The potential and spectroscopic parameters needed to use the above potential energy are listed in Table 1.[29-33] The Sato parameters modify the potential in the interaction region, where the energy barrier is known to be in the range of 0.4-1.2 kcal/mole.[34] Making Δ_{II} negative gives the desired effect of moving the exothermicity into the exit channel. Using the potential parameters listed in Table 1, the best potential energy surface exhibiting no minimum in the product valley and producing the barrier height that is closest to the known range is found when we set the Sato parameters for H_3C-I_A, H_3C-I_B and I-I to +0.10, +0.10, 0.15, respectively. We have varied the Δ_i's to some extent and found that, although this causes some change in reaction probabilities, the principal qualitative features of this study remain unchanged. Figure 2 shows the resulting PES for $\Xi = 0°$, where the barrier occurs at the

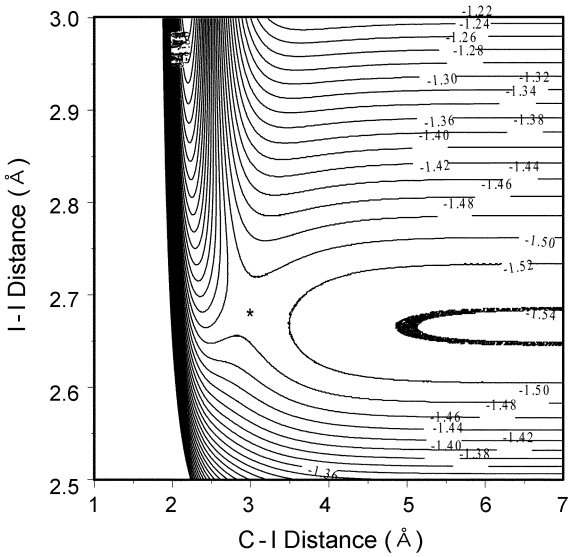

Figure 2. Potential energy surface for $\Xi = 0°$. The contours are labeled in eV. The position of the barrier occurring at −1.51 eV is indicated by a star. The curves are in 0.02 eV interval.

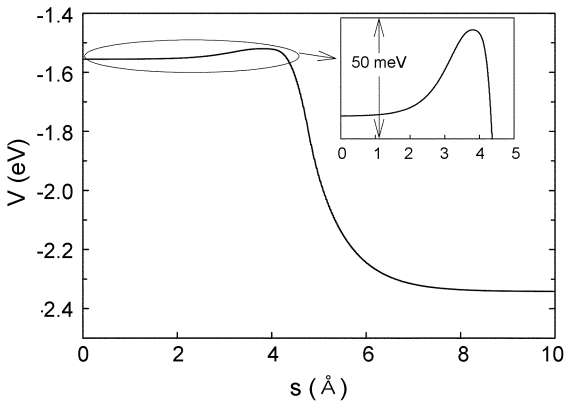

Figure 3. Minimum energy path (MEP) for the title reaction; s is the reaction coordinate. Full line: potential along the MEP. The inset shows the enlarged energy barrier in the entrance valley.

H_3C-I distance of 3.0 Å and the I-I distance of 2.7 Å, which represent an early barrier in the entrance valley. For this Ξ, the barrier height is 29.9 meV. This barrier is shown in Figure 3, which is the potential along the MEP as a function of the intrinsic reaction coordinate s.[35] Significant alterations of the collision geometry result in changes in the PES. When Ξ is changed toward ± 45°, the height and location of the saddle point begin to change somewhat, but the major features of the PES remain unchanged. However, beyond this Ξ range, the PES changes significantly from the $\Xi = 0°$ case, shifting the saddle point toward the exit valley, in which case the reaction exoergicity goes preferentially into translation. The majority of the molecules produced in low-lying vibrational levels are from such reactive events.

Equations of Motion

The interaction potential energy given by Eq. (3) is dependent on the pertinent coordinates as U (r, θ, ϕ, Z, Γ, x_1, x_2, x_3, δ_{12}, δ_{23}, δ_{31}, ρ). Thus, we set up the equations of motion $\mu_i(d^2q_i/dt^2) = -(\partial U/\partial q_i)$ for $q_1 = r$, $q_2 = \theta$, $q_3 = \phi$, $q_4 = Z$, and $q_5 = \Gamma$ where μ_i represents the corresponding reduced mass (m_r, m_R) or moment of inertia I. For the C-H_i stretching and H_i-C-H_j bending motions, the equations are $\mu_{CH}(d^2x_i/dt^2) = -(\partial U/\partial x_i)$, where i = 1, 2, 3, and $\mu_\delta(d^2\delta_{ij}/dt^2) = -(\partial U/\partial\delta_{ij})$, where ij = 12, 23, 31. The equation of motion of the ρ rotation is $I_{CH_3}(d^2\rho/dt^2) = -(\partial U/\partial\rho)$. Here μ_{CH} and μ_δ are the reduced masses associated with the CH vibration and the H_i-C-H_j bending, respectively, and I_{CH_3} is the moment of inertia of the CH_3 rotation.

We solve the equations of motion by using standard numerical procedures for initial conditions ($t = t_0$):

$$r(t_0,E^0_{v,I_2},\xi_{I_2})=2a_{II}\ln\{[1+(E^0_{v,I_2}/D_{II})^{1/2}\times\sin(\Lambda_{I_2}t_0+2\pi\xi_{I_2})]/[1-(E^0_{v,I_2}/D_{II})]\}, \quad (5a)$$

$$\theta(t_0,J,\xi_\theta) = [J(J+1)]^{1/2}(\hbar/I)t_0 + 2\pi\xi_\theta, \quad (5b)$$

$$\phi(t_0,J,\xi_\phi) = [J(J+1)]^{1/2}(\hbar/I)t_0 + 2\pi\xi_\phi \quad (5c)$$

$$Z(t_0,E) = Z_e + a\ln[(D_{CI}/E)+(D_{CI}/E)^2] + 2a\ln\{\cosh[(E/2\mu)^{1/2}(t_0/a)]-[D_{CI}/(E+D_{CI})]^{1/2}\}, \quad (5d)$$

$$\Gamma(t_0) = b \quad (5e)$$

$$x_i(t_0,E^0_{v,CH,i},\xi_i) = 2a_{CH}\ln\{[1+(E^0_{v,CH,i}/D_{CH})^{1/2}\times\sin(\Lambda_{CH}t_0+2\pi\xi_i)]/[1-(E^0_{v,CH,i}/D_{CH})]\}, \quad i = 1, 2, 3, \quad (5f)$$

$$\delta_{ij}(t_0,\xi_{ij}) = \frac{2}{3}\pi\sin[(k/\mu_\delta\lambda^2)^{1/2}t_0+2\pi\xi_{ij}], \quad ij = 12, 23, 31 \quad (5g)$$

$$\rho(E_R, t_0, \xi_{CH_3}) = (2E_R/I_{CH_3})^{1/2} t_0 + 2\pi\xi_{CH_3}, \quad (5h)$$

where E is the collision energy, $\Lambda_{I_2}=[(D_{II}-E^0_{v,I_2})/2\mu_{I_2}]^{1/2}/a_{I_2}$, E^0_{v,I_2} is the initial vibrational energy of I_2, and E_R is the energy associated with the ρ-rotation of CH_3. Similarly, $\Lambda_{CH}=[(D_{CH}-E^0_{v,CH,i})/2\mu_{CH}]^{1/2}/a_{CH}$, $E^0_{v,CH,i}$ is the initial energy of the C-H vibration. In Eq. (5g), k/l^2 is the force constant of the bending vibration and μ_δ is the associated reduced mass (see Table 1). Randomly sampled are the impact parameter $b = b_{max} \geq b$, where b_{max} is the maximum value of b, the initial vibrational phase ($2\pi\xi_{I2}$) and the rotational phases ($2\pi\xi_\theta$, $2\pi\xi_\phi$) of I_2, the CH vibrational phase $2\pi\xi_i$, the initial H_i-C-H_j vibrational phase $2\pi\xi_{ij}$, and the initial phase $2\pi\xi_{CH_3}$ of the CH_3 rotation, where ξ is a random number with a flat distribution in the closed interval (0, 1). We use the rotational and vibrational distribution functions $g_n(2J+1)\exp[-J(J+1)\hbar^2/2IkT_{I_2}]/Q_r$ and $\exp[-(v+1/2)\hbar\omega/kT_{I_2}]/Q_v$ to sample J and v of I_2, respectively, at a given iodine source temperature T_{I_2}. We then determine the initial rotational and vibrational energies ($E_{r,0}$, $E_{v,0}$) corresponding to these quantum numbers. Here, g_n is the nuclear spin statistical weight, and Q_r, Q_v are the rotational and vibrational partition functions, respectively. For CH_3, we sample the initial vibrational energies for three C-H stretchings and three H-C-H bending modes. Finally, we assume the distribution of incident velocities of the methyl radicals to be Maxwellian at the methyl radical temperature T_{CH_3}.

Results and Discussion

A. Reaction Probability. We carry out the integration of the equations of motion for each of the 30,000 sets of the initial conditions defined above. We regard the initial rotational phases expressed as $2\pi\xi_\theta$ and $2\pi\xi_\phi$ in Eqs. (5b) and (5c) to describe orientation of the target molecule at the instant when the radical enters the interaction region (*i.e.*, at $t = t_0$). In particular, the values of θ_0 and ϕ_0 can be used to determine the deviation of the collision geometry from the collinear configuration of $H_3C\cdots$I-I at the instant for a given value of b. The molecule then undergoes its rotational motion from this initial orientation with the angular velocity $(\hbar/I)[J(J+1)]^{1/2}$, which is the result obtained by equating the classical energy expression to the quantal expression. The collinear geometry can also be described by the orientation angle Ξ for an arbitrary value of b. We have made a series of runs in the neighborhood of $b = z_{CH_3-I,e}+r_{I-I,e} = 3.472$ Å to determine the maximum value of b (*i.e.*, b_{max}), which is sufficiently large such that no reaction takes place for $b \geq b_{max}$. It is found to be 4.0 Å.

We regard the I_2 dissociation to have occurred when the bond displacement exceeds the equilibrium bond distance by 5 Å (*i.e.*, the I to I distance of 2.666 Å + 5.000 Å = 7.666 Å) and the C-I distance remains in the range of ($z_{CH_3-I,e}$ − 0.289) Å to ($z_{CH_3-I,e}$ + 0.861) Å. We have established this range of the C-I distance by repeated sampling of reactive trajectories. At the instant of product (say CH_3I_A) formation,

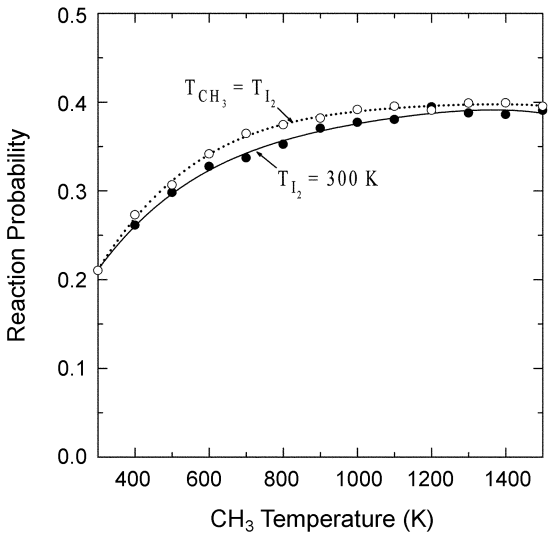

Figure 4. Temperature dependence of reaction probabilities P. The upper curve (open circles) is for the probability as a function of $T_{CH_3}=T_{I_2}$. The lower curve (filled circles) represents the dependence on T_{CH_3} for T_{I_2} fixed at 300 K.

we switch the numerical procedure from the integration of the above equations to the integration of the equation of motion for the $CH_3\cdots I_A$ coordinate, the procedure which is equivalent to matching the wavefunction between the entrance and exit channel in quantum dynamics procedures. We start the integration of the complete set of the equations of motion from the initial separation of 15 Å between CH_3 and I_2 for the initial conditions specified by Eq. (5) and follow each trajectory for 100 ps. Although reactive events occur on a much shorter time scale, we choose this long time to ensure that no trapped trajectories are present and no recombination of iodine atoms occurs. We are mainly concerned with the reaction taking place at T_{CH_3} = 1000 K and iodine molecules at T_{I_2} = 300 K, but the study will be extended to 300 K ≤ T_{CH_3} ≤ 1500 K for T_{I_2} fixed at 300 K and to 300 K ≤ $T_{CH_3} = T_{I_2}$ ≤ 1500 K for a brief discussion of the temperature dependence. For convenience, we specify each thermal condition as (T_{CH_3}, T_{I_2}).

We first consider the temperature dependence of the reaction probability P, which is defined as the ratio of the number of reactive trajectories N_R to the total number N_0 sampled. We display the dependence in Figure 4 for the two sets. One of them is the dependence of P on the temperature of the CH_3 source, which has been varied between 300 K and 1500 K, for the temperature of the I_2 source maintained at 300 K. The other set is the dependence of P on both CH_3 and I_2 temperatures, which have been set equal to each other and varied from $T_{CH_3} = T_{I_2}$ = 300 K to 1500 K. When the I_2 source temperature is fixed at 300 K, the dependence of the reaction probability on T_{CH_3} first increases from 0.210 at 300 K to 0.370 at 900 K, beyond which it remains nearly constant as temperature increases. At T_{CH_3} = 1500 K, the reaction probability is 0.390. For $T_{CH_3} = T_{I_2}$, the probability is somewhat higher than the above case where T_{I_2} is fixed at 300 K, and the dependence is also week. At 300 K it is 0.210

and rises to 0.391 at 1000 K, after which it remains nearly constant to 0.395 at 1500 K.

From the temperature dependence shown in Figure 4, we choose the thermal conditions T_{CH_3} = 1000 K and T_{I_2} = 300 K for a detailed study of the reaction throughout the following sections. At these conditions, the reaction probability is 0.378, which is slightly higher than that (0.342) of the previous model in which the effect of hydrogen atoms are not included.[13] Our choice of 1000 K of CH_3 for the main part of the study is motivated partly by the experimental conditions of 800-1500 K used by other researchers.[11] In these experimental studies, methyl radicals were prepared by thermal decomposition of $(CH_3)_2Zn$ or $(CH_3)_2Cd$, and temperatures at which iodine beams were prepared are in the range of 400-435 K. At 1000 K, the relative velocity of the collision partners is 1.32×10^3 m/sec, but we use a thermal distribution of collision energies rather than a single value of the energy such as the most probable energy.

When we set the initial vibrational energy of I_2 equal to the v = 0, 1, and 2 levels, the reaction probability at T_{CH_3} = 1000 K is 0.373, 0.378, and 0.386, respectively. This insensitivity is primarily due to a low barrier height (0.4-1.2 kcal/mol or 140-420 cm^{-1}) as an increase in the initial vibrational energy does not significantly affect the reaction which is already efficient at T_{CH_3} = 1000 K (or 1040 cm^{-1}). For I_2, the vibrational quantum $\hbar\omega_{I_2}$ is only 214.5 cm^{-1}.

The dependence of reactive events on the impact parameter is shown in Figure 5. To determine the dependence of the extent of reaction on the impact parameter b, *i.e.*, the opacity function $P(b)$, we count reactive trajectories in b = 0.05 Å interval and divide that number by the number of collisions taking place in the same interval. For example, between b = 0.10 and 0.15 Å, the number of trajectories sampled is $N(b)$=215, of which $N_R(b)$=162 are reactive. The opacity function $P(b)=N_R(b)/N(b)$=0.754 is plotted at the midpoint of the range, b=0.125 Å in Figure 5. (We note that the total number of trajectories sampled between b=0 and b_{max} is N_0=30,000.) The probability defined in the previous paragraph is the ratio of the total number of reactive trajectories to the ensemble size N_R/N_0, *i.e.*, a total reaction probability. The opacity function is the largest near b=0 and then decreases slowly with increasing b to b=2.0 Å. The plot shows that although it decreases rapidly with increasing impact parameter after b=2.0 Å, the reaction is efficient over a wide range of b. Even at b as large as $z_{CH_3-I,e} + r_{I-I,e}$ = 3.472 Å, the opacity is about 0.10. The reaction finally ceases when b > 4 Å. The total reaction cross-section defined as

$$\sigma_R = 2\pi \sum_0^{b_{max}} P(b)bdb = 2\pi \sum_0^{b_{max}} \frac{N_R(b)}{N(b)} bdb \qquad (6)$$

is found to be as large as 16.1 $Å^2$ for this efficient reaction at T_{CH_3} = 1000 K and T_{I_2} = 300 K. At T_{CH_3} = 300 K, the cross section is 7.91 $Å^2$ and increases to 15.8 $Å^2$ at 900 K. The cross section remains constant near 16 $Å^2$ for T_{CH_3} > 900 K. In their molecular beam study of CH_3+I_2 at the radical temperature of 1500 K and the iodine reservoir temperature at 403 K, McFadden *et al.* have reported the total cross section σ_R = 5.0 $Å^2$ with uncertainties of a factor of three.[11] Note that the relative velocity of their reactants was 1.65×10^3 m/s, as compared to the room temperature velocity of 7.23×10^2 m/s. When we extend the present calculation to the thermal conditions of (1500, 403 K), the total cross section is 16.7 $Å^2$, which is near the upper end of the uncertainty range of the McFadden data. Here we have used the Boltzmann distribution of the initial vibrational energy of I_2 at 403 K. The calculated total cross sections are in the range of estimated values 5-20 $Å^2$ for halogen atom-molecule reactions such as Br+I_2 and Cl+Br_2.[36]

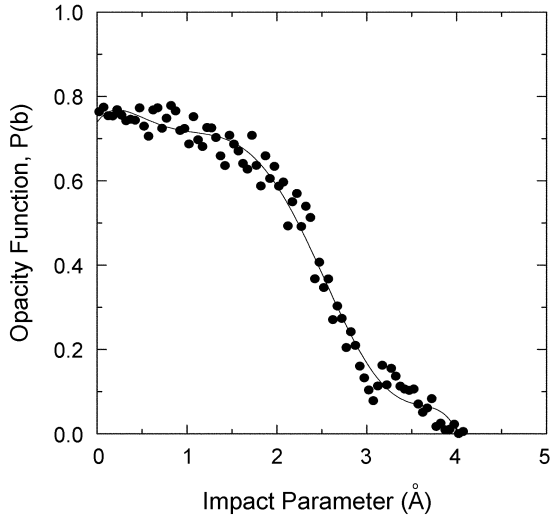

Figure 5. Dependence of the opacity function $P(b)$ on the impact parameter at T_{CH_3} = 1000 K and T_{I_2} = 300 K.

Before closing this section, we note that there is another reaction pathway in addition to the CH_3I formation, *i.e.*, I_2 dissociation without any $H_3C\cdots I$ bond formation. The probability of the I_2 dissociation reaction without $C\cdots I$ bond formation is 0.006. The I_2 dissociation occurs mostly in large-b collisions and the $H_3C\cdots I$ bond formation reaction is not efficient in such collisions, indicating that the distance between CH_3 and I_2 is too far for a concerted mechanism to prevail.

B. Product Energy Distribution. The energy of CH_3 to I attraction is 54.5 kcal/mol (2.36 eV) and the I-I dissociation energy is 35.9 kcal/mol (1.56 eV). Thus, there is a significant difference between the energy originally stored in the bond that is broken and the methyl radical to iodine atom attractive energy. It is this difference (*i.e.*, the excess energy) that controls the extent of product excitation. After dissociating the I_2 bond, the major portion of this difference at E sampled at T_{CH_3} = 1000 K is found to deposit in the translational motion and the H_3C-I vibrational motion of the product molecule. The ensemble-averaged translational energy of CH_3I and energy of the H_3C-I vibration are 0.68 eV and 0.29 eV, respectively. This distribution indicates that a significant amount of acceleration of the trajectory occurs

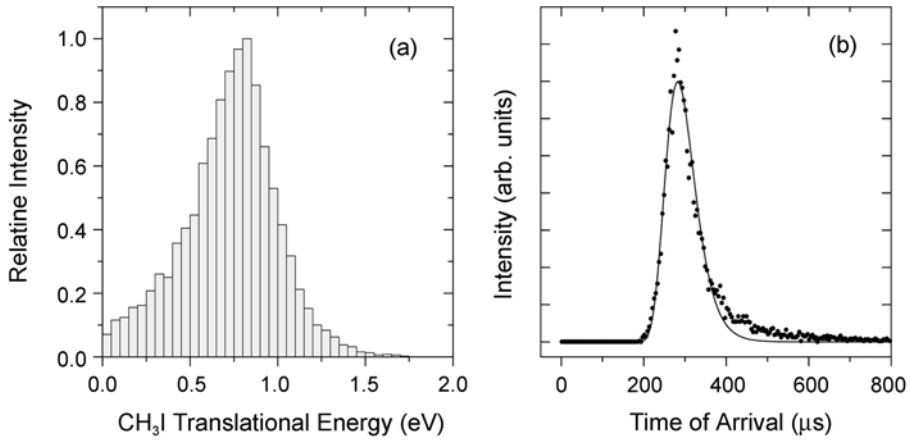

Figure 6. (a) Product CH_3I translational population distribution. (b) Time of arrival distribution of the CH_3I product. The curve shows the result of a fit to $f(v) \propto v^3\exp[-(v-v_0)^2/\kappa^2]$. Both figures are at T_{CH_3} = 1000 K and T_{I_2} = 300 K.

before and after turning the corner of the $CH_3\cdots I$ impact point, resulting in the acceleration of the vibrational coordinate, which feeds energy continuously out of the translational motion before $CH_3\cdots I$ stabilizes to the final CH_3I.

As shown in Figure 6a, the translational population distribution is shifted to higher energy side compared to the Maxwell distribution, its peak being shifted to $\cong$ 0.7 eV, which is far above that expected from the thermal conditions (1000, 300 K). From the translational energy distribution, we can obtain information on the velocity distribution of outgoing CH_3I product molecules, assuming a distance of 30 cm for the molecule to travel from the reaction zone to the "detector". In Figure 6b, we plot the time-of-flight distribution of CH_3I at (1000, 300 K). The fit assumes that CH_3I has the velocity distribution of the form $f(v) \propto v^3 \exp[-(v-v_0)^2/\kappa^2]$,[37] where a best fit yields v_0=1008 m/s and κ =195 m/s. The most probable arrival time is 282 μs with the velocity close to v_0. That is, the maximum of the velocity distribution occurs at a velocity which is far greater than the velocities corresponding to the thermal conditions of (1000, 300 K). This highly non-Maxwellian distribution of product translation reflects the situation that the reaction energy deposits preferentially in the translational motion when the molecule is produced in a low-lying vibrational state.

The distribution of the excess energy deposited in the CH_3-I vibration is as shown in Figure 7a. From the eigenvalue expression $E_{vib}(v) = hc\omega_e(v + ½) - hc\omega_e x_e(v + ½)^2$ for the CH_3-I vibration, with ω_e=533 cm^{-1} [30] and the anharmonicity constant $\omega_e x_e = 3.80$ cm^{-1} estimated from a standard expression,[38] we find $E_{vib}(0)$=0.033 eV and $E_{vib}(1)$=0.099 eV. About 15% of the product molecules have their CH_3-I vibrational energy in the $E_{v,C\text{-}I}$ range of 0 to 0.05 eV, which includes $E_{vib}(0)$. Nearly 13% of the product molecules are in the range between 0.05 and 0.10 eV, which includes the v=1 state. However, Figure 7a shows that about one-third of CH_3I molecules produced in the reaction have their CH_3-I vibrational energy above 0.35 eV, which corresponds to $v \geq 5$, indicating the accumulation of a significant portion of the exothermicity in product vibration. The fraction of CH_3I with vibrational energy as high as or greater than 1 eV is about 3%. The eigenvalue expression gives $E_{vib}(17)$=1.01 eV. A clearer presentation of this efficient vibrational excitation is shown in Figure 7b, where

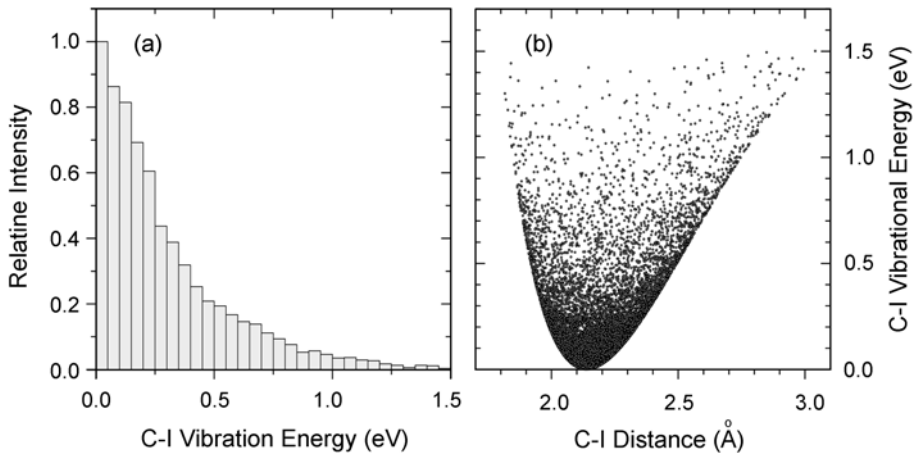

Figure 7. (a) Product H_3C-I vibrational population distribution. (b) Plot of the H_3C-I vibrational energy versus the H_3C-I bond distance. Both figures are at T_{CH_3} = 1000 K and T_{I_2} = 300 K.

the H_3C-I vibrational energy is plotted against the C-I bond distance for all reactive events. Here we determine the H_3C-I bond distance of all reactive events at the instant when the receding CH_3I has reached the fixed value of 30 Å from the reaction zone. At any instant, the H_3C-I distance of each CH_3I takes a value between the two turning points around the equilibrium bond distance 2.139 Å. This plot shows that the CH_3-I bond lengths are concentrated at the turning points of vibrational amplitudes, an important feature predicted by classical mechanics. A high concentration of reactive events at the turning points is especially apparent between the vibrational energy 0.3 and 0.9 eV, but above this range, there are not enough reactive events to manifest the effect. Results similar to these shown in Figure 7b have been found in the vibrational distribution of OH radicals produced in the reaction of atomic oxygen with chemisorbed hydrogen atoms on a tungsten surface.[28] This distribution, when compared with that of translational energies, suggests that the vibrational and translational energies are anti-correlated.

C. Reaction Dynamics. We find a new class of reactive trajectories which was not found in the previous report.[13] The number of such trajectories is small (1,193 out of 30,000 sampled) and these reactive events occur in the forward direction, which is below the xy plane sketched in Figure 1. This situation occurs when CH_3 first interacts with I_2 in the reaction zone, while undergoing a large amplitude motion. The product molecule then emerges from the reaction zone into the forward hemisphere. In all of the reactive events reported in Ref. 13, the formation of CH_3I occurs in the backward direction, where the product has bounced backward after the impact. Thus, in the collision model employed in Ref. 13, the reactive events occur above the xy plane defined in Figure 1. We include all these forward and backward reactive events in the present calculation.

At the thermal conditions of (1000, 300 K), 90% of 11,332 reactive events occur on a sub-picosecond time scale. The ensemble average of all reactive trajectories gives an average reaction time of 0.36ps. Here the reaction time t_R is defined as the time required for CH_3I to form after the initial impact (see below). Some reactive events occur at the reaction time as long as 5 ps or longer, but the number of such events is negligible. From a detailed analysis of reactive trajectories, we find that CH_3I is produced either in the space above or below the xy plane shown in Figure 1 as noted in Section A. In the former type, the incident radical collides with I_2 and then bounces backward with one of the iodine atoms almost always on a sub-picosecond scale. In fact, Figure 8 shows that nearly all of the sub-picosecond events occur above the xy plane (*i.e.*, in the backward hemisphere). On the other hand, in the latter type, CH_3 travels forward through the target and attracts one of the iodine atoms on the way out from the reaction zone in the forward direction, thus forming CH_3I in the space below the xy plane (*i.e.*, in the forward hemisphere). As shown in the right panel of Figure 8, a small fraction of the reactive events (1,193 out of 11,332 reactive trajectories) belongs to this

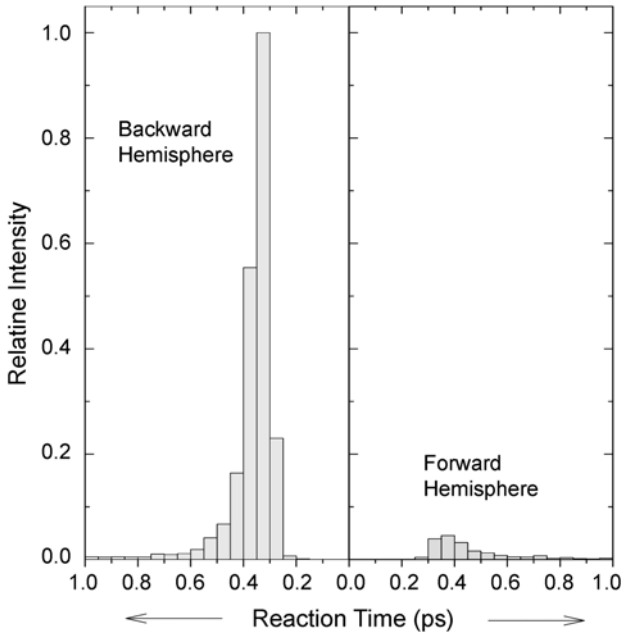

Figure 8. Distribution of reaction times at T_{CH_3} = 1000 K and T_{I_2} = 300 K for reactive events taking place in the backward and forward hemisphere. Those events which occur on a subpicosecond scale are shown.

type. Thus, the reaction time of these events is somewhat longer than that of backward rebounding events. Although it is not shown in Figure 8, we find that about one-third of these forward events occurs on a picosecond time scale ($t_R >$ 1ps). In these long-time events, CH_3 forms a long-lived complex $CH_3\cdots I\cdots I$ undergoing a large amplitude motion in the reaction zone before forming CH_3I in the forward hemisphere. A small fraction of the backward reactive events also occurs on a picosecond scale. From the backward reactive events, Figure 8 shows that no reaction occurs until the reaction time of about 0.2 ps after the impact. After this "incubation" period, there is a sudden burst of reactive events, reaching the maximum intensity in a matter of about 0.3 picosecond. Beyond this time, the intensity decreases exponentially. On the other hand, for the forward reactive scattering, the I_2 vibration is not a spectator because the I_2 bond dissociates and the new $H_3C\cdots I$ bond is produced.[39] But, the energy of the $H_3C\cdots I$ bond produced in the forward scattering is smaller than that of the backward scattering.

The rate constant of the present system is calculated as 3.92×10^{-12} $cm^3\cdot molecule^{-1}\cdot s^{-1}$. An activated complex calculation by Johnston and Goldfinger predicted a rate constant of 1.8×10^{-14} $cm^3\cdot molecule^{-1}\cdot s^{-1}$ for the reaction of CH_3 with Cl_2.[40] Bell *et al.* used a molecular orbital-bond index and group method to calculate a rate constant of 5.8×10^{-11} $cm^3\cdot molecule^{-1}\cdot s^{-1}$ for the latter reaction.[41] In the quantum mechanical study of the reaction of methyl radicals with chlorine molecules, Drougas *et al.* reported that the rate constant is 2.15×10^{-12} $cm^3\cdot molecule^{-1}\cdot s^{-1}$ at 300 K.[14(a)] Kovalenko and Leone measured the rate constants of the analogous reactions $CH_3 + Br_2 \rightarrow CH_3Br + Br$ and $CH_3 +$

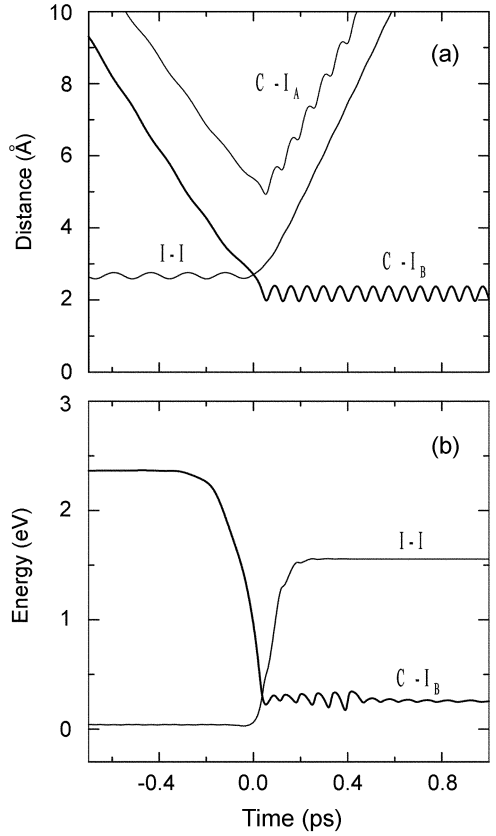

Figure 9. Dynamics of the typical short-time reactive event at T_{CH_3} = 1000 K and T_{I_2} = 300 K. (a) Time evolution of the H_3C-I_A. H_3C-I_B and I-I distances. (b) Time evolution of the H_3C-I_B and I-I interaction energies.

$Cl_2 \rightarrow CH_3Cl + Cl$ at 800 K as $2.0(\pm 0.4) \times 10^{-11}$ and $1.54(\pm 0.11) \times 10^{-12}$ $cm^3 \cdot molecule^{-1} \cdot s^{-1}$, respectively.[4] Thus, the present result is comparable with theoretical and experimental results.

We now look into the detailed dynamics of these short-time and long-time events. To discuss dynamical features of short-time events, we select a reactive case which best represents the ensemble of sub-picosecond processes displayed in Figure 8. It is from the backward rebound type and the results are shown in Figure 9. We first note that an important time scale in collision dynamics is the collision time (*i.e.*, the duration of collision). Evaluation of this time scale is not a trivial matter because it is often difficult to determine when the interaction begins and ends. As shown in Figure 9a, it does not appear possible to determine the start of collision from the time dependence of the I-I or H_3C-I distances. On the other hand, the start of collision is clearly noticeable in the evolution of the H_3C to I_B interaction energy, $E_{v,C-I_B}$, shown in Figure 9b. (Note that Figures 9a and 9b are plotted on the same time scale.) The decrease of this interaction energy from the initial value $D_{C\text{-}I}$ is noticeable near t = –0.30 ps. Therefore, we consider the collision to have started at this instance in the time frame of numerical integration employed in the present study. In all collisions considered in this study, we find $E_{v,C-I_B}$ starts to decrease from $D_{C\text{-}I}$ at t = –0.30 ps. The energy buildup in the I-I bond ($E_{v,I\text{-}I}$) occurs immediately after the decrease of $E_{v,C-I_B}$. From Figures 9a and 9b, it is obvious that H_3C and two iodine atoms are in the close range of one another for a brief period. Even so, we can think of the formation of a short-lived complex $H_3C \cdots I \cdots I$. The sharp variation of the curves shown in Figure 9b suggests that there is a rapid flow of energy from the $H_3C \cdots I$ bond to the I-I vibration in $H_3C \cdots I \cdots I$ as a result of the short-range interaction between C and I atoms and that these energy loss and buildup processes in the complex occur rapidly before the complex has had a chance to disintegrate. The efficient energy buildup in the I-I bond leads to the I-I dissociation and the CH_3I formation. Thus, in this short-time reactive event, the transfer of a large amount of energy (>> kT) occurs in a single step, the mechanism which is similar to that considered in the basic RRKM model of unimolecular decomposition processes, where the processes of activation and deactivation are treated as essentially single-step processes as opposed to the ladder-climbing processes in which molecules acquire or lose their energy in a series of small steps.[42]

As the reactant state goes through the low barrier on the PES shown in Figure 2, the early release of attractive energy appears initially as kinetic energy in the $C \cdots I$ direction[43,44] followed by energy buildup in the I-I vibration. This energy buildup process is very efficient near t = +0.05 ps, at which time CH_3 approaches close to I_2 for the first impact (see the C-I_B distance in Figure 9a). Upon impact, I_2 gains a large amount of energy in its vibrational motion and the distance of the weakened I-I bond begins to diverge, eventually reaching the I to I distance of 7.67 Å at t = +0.42 ps. After passing through the barrier, the short-range repulsion between H_3C and I eventually converts the reaction exoergicity into product vibration. At t = +0.42 ps, the H_3C and I_B distance begins to undergo a highly regular oscillation, while the C-I_A distance diverges. The highly organized oscillation of the H_3C-I_B distance beyond t = +0.42 ps indicates the formation of a stable CH_3I_B in an excited vibrational state as it bounces backward from the reaction region. Beyond t = +0.42 ps, the H_3C-I_B interaction energy shown in the figure now represents the vibrational energy of the newly formed H_3C-I_B bond in CH_3I_B and is 0.25 eV, which is very close to the v = 4 energy level obtained from the eigenvalue expression. In this representative case, therefore, the time spent by the collision partners in the interaction region from the start of collision at t = –0.30 ps to the end of interaction at t = +0.42 ps when the products fly apart is 0.72 ps, which is the duration of collision. However, the reactive event really begins at the first impact, which occurs at t = +0.05 ps, and continues until t = +0.42 ps, when the product is formed. That is, the reaction time for this representative trajectory is 0.37 ps.

As the first impact occurs, the I-I bond gains a large amount of energy from the incident radical. During the reaction period following the impact, the internal motion of $CH_3 \cdots I \cdots I$ redirects sufficient energy along the weakened I-I vibration and leads to the I-I dissociation and the H_3C-I

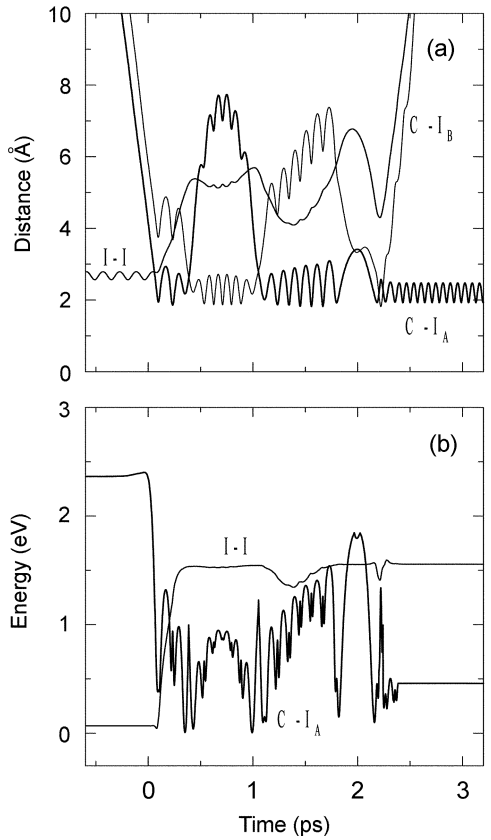

Figure 10. Dynamics of the typical long-time reactive event at T_{CH_3} = 1000 K and T_{I_2} = 300 K. (a) Time evolution of the H_3C-I_A, H_3C-I_B and I-I distances. (b) Time evolution of the H_3C-I_B and I-I interaction energies.

bond formation. Figures 9a and 9b show that the vibrational energy of I_2 rises to the dissociation threshold at a time about 0.2 ps before the I-I bond distance reaches the critical value of 7.67 Å for dissociation.[13] The stabilization of the $H_3C\cdots I_B$ complex to CH_3I_B occurs during this period, where the short-range $H_3C\cdots I_B$ repulsion converts the exoergicity into the H_3C-I_B vibration. We have checked many reactive trajectories and found that, although time scales differ for different trajectories, the qualitative behavior for all short-time trajectories remains unchanged with a time lag of 0.2 to 0.3 ps for the collision partners then take 0.3-0.5 ps to form CH_3I in all these short-time collisions. In the reverse-process of $CH_3I+I \rightarrow CH_3+I_2$, Zewail and his collaborators have shown that the time scale for the C-I dissociation of CH_3I is as short as 0.15 ps.[12]

In a reactive event taking place on a picosecond (long-time) scale, the collision partners form a long-lived complex before reaching the exit channel. Although such collisions are infrequent, they represent an interesting class of reactive events in the present system. Figure 10 shows the case representing the reactions that occur on this long-time scale. We have selected it from those reactive events that have occurred in the forward hemisphere. As noted above, larger fraction of long-time reactive events comes from this region than in the backward rebound type. Until the first impact, the time evolution of the methyl radical to iodine distances and the I-I bond distance is very similar to the short-time case considered in Figure 9a, but beyond the initial stage, the time evolution becomes much more complicated. The time evolution of the iodine bond distance shows that the rebounding iodine atoms spend a relatively long time near the apex of the bound trajectory, where the kinetic energy vanishes, but the I-I bond fails to dissociate (see Figure 10a). In this trajectory, the initial rotational level of I_2 is J = 137, and the rotational velocity at this J is 1.936 rad/ps, which corresponds to the classical rotation time of 3.25 ps. Even though I_2 cannot rotate within ~1 ps with this rotational energy, I_2 rotation is accelerated after the first impact, because the rotational energy as well as the vibrational energy of I_2 are activated. Thus, in the $CH_3\cdots I_2$ complex the I_2 becomes to rotate rapidly. As a result, as shown in Figure 10a, the $CH_3\cdots I_A\cdots I_B$ complex is changed to $CH_3\cdots I_B\cdots I_A$, and to $CH_3\cdots I_A\cdots I_B$ again by this rapid rotation (within ~1 ps). After large amplitude oscillations, the iodine molecule finally dissociates near t = +2.3 ps. The incident methyl radical becomes bound to the I_A end of the iodine molecule immediately following the initial impact, and after a long period the complex $H_3C\cdots I_A\cdots I_B$ finally leads to the product CH_3I_A. The variation of the H_3C-I_A (dark) and H_3C-I_B (light) curves shown in Figure 10a clearly indicates that when CH_3 is bound to I_A, I_B undergoes a large amplitude oscillation and is unable to come within close range of CH_3 for the C-I_B formation or vice versa in a triangular configuration of CH_3 to the two iodine atoms. In such a triangular shape, one of the two iodine to carbon distances is much longer than the other, forming a nearly linear configuration along $H_3C\cdots I_A\cdots I_B$ (an obtuse triangle).

Figure 10b shows a rapid rise of the I-I vibrational energy toward the dissociation threshold as the H_3C-I attractive interaction decreases sharply from $D_{C\text{-}I}$. This variation is very similar to the short-time case considered in Figure 9b, but beyond the initial stage, the time evolution is radically different from that of the short-time case. The H_3C to I_A interaction energy rapidly oscillates in the complex state $H_3C\cdots I_A\cdots I_B$. Comparing Figure 10b with Figure 10a, we find that the I-I bond gains essentially all the energy needed to dissociate during the brief period of the first round trip while CH_3 is bound to I_A. Therefore, the decision to produce CH_3I_A is made at the very early stage of collision in this long-time reactive event. It is interesting to find in Figure 10a that I_B approaches close to CH_3 for a brief period, but is quickly pushed out by I_A. The frustrated I_B reaches close to the radical one more time near t = +2 ps before becoming permanently repelled by $H_3C\cdots I_A$, which finally stabilizes to the product molecule with 0.458 eV in the C-I vibration at t = +2.3 ps.

D. Dependence of Reaction on the Initial Orientation of I_2. The most populated rotational level of I_2 at 300 K is J^* = 46. The rotational velocity $(\hbar/I)[J(J+1)]^{1/2}$ at $J = J^*$ is 0.655 rad/ps, which corresponds to the classical rotation time of 9.60 ps. Therefore, the rotation time is much longer than reaction times displayed in Figure 8. Note that the

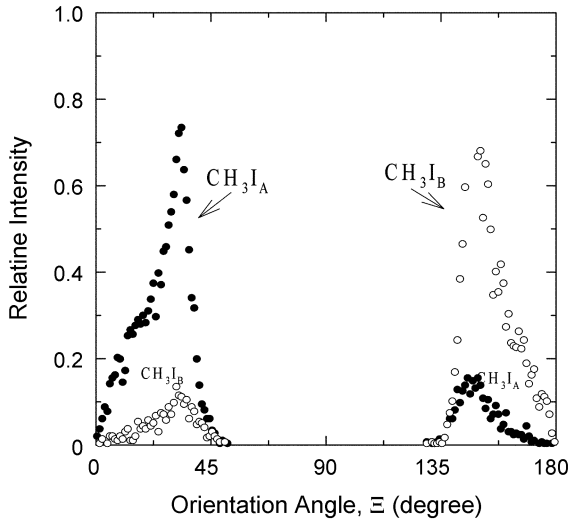

Figure 11. Distribution of reactive events for the orientation angle Ξ at T_{CH_3} = 1000 K and T_{I_2} = 300 K. The filled circles are for the intensity of CH_3I_A and the open circles are for the intensity of CH_3I_B.

vibrational period of I_2 is only 0.16 ps. It takes only about 0.2 ps for the incident radical to reach the turning point after entering the interaction region. For example, for the representative case shown in Figure 9, the collision time is about 0.6 ps, whereas the reaction time is about 0.4 ps, which is very short compared to the rotation time. Thus, these times suggest that the heavy target molecule will not rotate significantly during the interaction period. When Ξ = 0° or 180°, the collision configuration of C and I_2 are aligned collinearly as $H_3C\cdots I_A\cdots I_B$ or $H_3C\cdots I_B\cdots I_A$, along which energy flow from the H_3C-to-I interaction to the I-I vibration is efficient, regardless of the value of impact parameter. The distribution of this angle at the instant of impact for all reactive events reveals useful information on the effects of molecular orientation on the reaction. In a short-time reaction, the iodine molecule dissociates and forms the product molecule at this angle. The plot of such a distribution shown in Figure 11 indicates that the distribution of reactive events is strongly dependent on Ξ. The significant scatter of reactive events seen in the figure is largely due to the distribution of initial rotational energies of I_2. The rotational distribution function contains the effects of nuclear statistics resulting from I=5/2, which lead to the total statistical weight of $(2I+1)I(2J+1)=15(2J+1)$ for even J and $(2I+1)(I+1)(2J+1)=21(2J+1)$ for odd J. Thus, we expect a rotational intensity alternation in the ratio 15:21. The formation of CH_3I_A is favored in the vicinity of the collinear configuration Ξ = 0°(or 360), whereas the formation of CH_3I_B occurs preferentially in the configuration Ξ = 180, clearly indicating that the process of reaction is over before I_2 has had time to undergo one or more rotations. Of course, the preference of CH_3I_A over CH_3I_B in the former vicinity (or *vice versa*) is entirely due to the choice of the coordinate system chosen in Figure 1. However, what is important is the occurrence of such preferential configurations for the reaction taking place essentially on a sub-picosecond scale. Thus, the formation of CH_3I_A through the near-collinear configuration of $CH_3\cdots I_A$-I_B occurs preferentially in one region of initial orientation, whereas CH_3I_B occurs through $CH_3\cdots I_B$-I_A in another region as shown in Figure 11. If the reaction process involves the formation of a complex with a lifetime long enough for I_2 to undergo many rotations in the reaction region, CH_3I_A or CH_3I_B would fly away in a random way with respect to the initial orientation of I_2, and there would be no such structured Ξ dependence. The I-I orientation ranges near 90 are dominated by the collisions in which CH_3 approaches I_2 perpendicularly, which is an unfavorable configuration for the vibrational excitation of I_2.

The intensities of the formation of CH_3I_A and CH_3I_B are sharply peaked at 30° and 150°, respectively. The main peak shown in Figure 11 represents the production of CH_3I_A or CH_3I_B in the backward hemisphere. The departure of the peaks from Ξ =0° is largely due to the situation that in the presence of strong attraction the CH_3 radical can react with the iodine atom before it has come to the hard-sphere contact (*i.e.*, at an angle smaller than the collinear angle Ξ =0°) for b smaller than $\frac{1}{2}r\sin\theta$. For b larger than $\frac{1}{2}r\sin\theta$, the reaction can occur at an angle larger than the collinear angle. For the Ξ =180° case for CH_3I_B, a similar situation occurs. Thus, except for the b=0 collision, the reaction is most likely to occur at an angle somewhat distorted from the collinear configuration as shown in Figure 11. Another interesting feature which can be observed in the figure is the appearance of a low intensity peak for CH_3I_A at 150° and that for CH_3I_B at 30°. These minor peaks are largely due to the reactive events that take place at long times, including those occurring in the forward hemisphere. Figure 11 shows that there is no reaction taking place in the intermediate angle range around 90°. The latter angle represents the T-shape configuration, which is inefficient for collision-induced energy buildup in the I-I bond. An interesting consequence of the result presented above is that we can readily determine branching ratios in an atom/radical+molecule reaction such as CH_3+AB forming CH_3A or CH_3B using the present procedure.

Concluding Comments

The present study shows that the majority of the reactive events of $CH_3 + I_2 \rightarrow CH_3I + I$ occur efficiently through direct-mode collisions on a subpicosecond scale over a wide range of impact parameters. The reaction probability is in the range of 0.3 to 0.4 and its temperature dependence is weak. In these short-time events, CH_3I molecules are produced on an early barrier PES with most of the exothermicity of the reaction deposited in the newly formed H_3C-I bond in CH_3I. More than one quarter of product molecules are shown to have the C-I vibrational energy which corresponds to several quanta or more. The amount of energy deposited in the CH_3I translational motion is significant and anticorrelated with the H_3C-I vibrational energy.

All reactive events are characterized by a sharp decrease of the $CH_3\cdots I$ interaction energy and a rapid buildup of vibrational energy in the I_2 bond at the very early stage of interaction.

Nearly all of subpicosecond reactive events occur in the backward hemisphere. The occurrence of these events is peaked around 0.36 ps. A small fraction of incident radicals travels through the target zone and produces CH_3I in the forward region. The interaction of CH_3 with $I_2(=I_AI_B)$ produces either CH_3I_A or CH_3I_B depending on the initial orientation of I_2, which does not change appreciably during the collision. Such anisotropic dependence of reactive events on molecular orientations suggests that the reaction is strongly favored when $H_3C\cdots I\cdots I$ is aligned collinearly and completes on a time scale much shorter than the rotational period of I_2.

Acknowledgment. This work was accomplished with research fund provided by Korean Council for University Education, support for 2004 Domestic Faculty Exchange. Computational time was provided by "the 6th Super-computing Application Support Program" of the KISTI (Korea Institute of Science and Technology Information).

References

1. Warnatz, J. *18th International Symp. Combustion*; Combustion Institute; Pittsburg, PA, 1981; pp 369-384.
2. Steinfeld, J. I.; Francisco, J. S.; Hase, W. L. *Chemical Kinetics and Dynamics*, 2nd Ed.; Prentice-Hall: Upper Saddle River, NJ, 1999; pp 516-524.
3. Scherer, J. J.; Aniolek, K. W.; Cernansky, N. P.; Rakestraw, D. J. *J. Chem. Phys.* **1997**, *107*, 6196.
4. Kovalenko, L. J.; Leone, S. R. *J. Chem. Phys.* **1984**, *80*, 3656.
5. Kawasaki, M.; Kasatani, K.; Sato, H.; Shinohara, H.; Nishi, N. *Chem. Phys.* **1984**, *88*, 135.
6. Tonokura, K.; Matsumi, Y.; Kawasaki, M.; Kasatani, K. *J. Chem. Phys.* **1991**, *95*, 5065.
7. Fan, Y. B.; Randall, K. L.; Donaldson, D. J. *J. Chem. Phys.* **1993**, *98*, 4700.
8. Suto, K.; Sato, Y.; Reed, C. L.; Skorokhodov, V.; Matsumi, Y.; Kawasaki, M. *J. Phys. Chem. A* **1997**, *101*, 1222.
9. Min, Z.; Quandt, R.; Bersohn, R. *Chem. Phys. Lett.* **1998**, *296*, 372.
10. Aitken, R. A.; Hodgson, P. K. G.; Morrison, J. J.; Oyewale, A. O. *J. Chem. Soc., Perkin Transactions* **2002**, *3*, 402.
11. McFadden, D. L.; McCullough, E. A., Jr.; Kalos, F.; Ross, J. *J. Chem. Phys.* **1973**, *59*, 121.
12. Zhong, D.; Cheng, P. Y.; Zewail, A. H. *J. Chem. Phys.* **1996**, *105*, 7864.
13. Ree, J.; Kim, Y. H.; Shin, H. K. *Chem. Phys. Lett.* **1997**, *272*, 419.
14. (a) Drougas, E.; Papayannis, D. K.; Kosmas, A. M. *J. Phys. Chem. A* **2002**, *106*, 6339; (b) *J. Mol. Struc.* (Theochem) **2003**, *623*, 211.
15. Suh, M.; Sung, W.; Li, G.; Heo, S.-U.; Hwang, H. J. *Bull. Korean Chem. Soc.* **2003**, *24*, 318.
16. Ree, J.; Chang, K. S.; Kim, Y. H.; Shin, H. K. *Bull. Korean Chem. Soc.* **2003**, *24*, 986, 1223.
17. Ree, J.; Kim, Y. H.; Shin, H. K. *Chem. Phys. Letters* **2004**, *394*, 250.
18. Ree, J.; Yoon, S.-H.; Park, K.-G.; Kim, Y. H. *Bull. Korean Chem. Soc.* **2004**, *25*, 1217.
19. Doepker, R. D.; Ausloos, P. *J. Chem. Phys.* **1964**, *41*, 1865.
20. Rice, J. K.; Truby, F. K. *Chem. Phys. Lett.* **1973**, *19*, 440.
21. Ting, C.-T.; Weston, R. E., Jr. *J. Phys. Chem.* **1973**, *77*, 2257.
22. Brown, L. C.; Whitehead, J. C.; Grice, R. *Mol. Phys.* **1976**, *31*, 1069.
23. Komaguchi, K.; Ishiguri, Y.; Tachikawa, H.; Shiotani, M. *Phys. Chem. Chem. Phys.* **2002**, *4*, 5276.
24. Kramer, K. H.; Bernstein, R. B. *J. Chem. Phys.* **1964**, *40*, 200.
25. Shin, H. K. *J. Phys. Chem.* **1971**, *75*, 923.
26. Buchachenko, A. A.; Gonzalez-Lezana, T.; Hernandez, M. I.; Delgado-Barrio, G.; Villarreal, P.; Stepanov, N. F. *Chem. Phys. Lett.* **1997**, *269*, 448.
27. Pattard, T.; Burgdorfer, J. *Phys. Rev. A* **2001**, *64*, 042720/1-042720/15.
28. Ree, J.; Kim, Y. H.; Shin, H. K. *J. Phys. Chem. A* **1997**, *101*, 4523.
29. Huber, K. P.; Herzberg, G. *Constants of Diatomic Molecules*; Van Nostrand Reinhold; New York, 1979; pp 330-332.
30. Herzberg, G. *Electronic Spectra and Electronic Structure of Polyatomic Molecules*; Van Nostrand; Princeton, 1967; Appendix VI.
31. Westre, S. G.; Liu, X.; Getty, J. D.; Kelly, P. B. *J. Chem. Phys.* **1991**, *95*, 8793.
32. Herzberg, G. *Infrared and Raman Spectra of Polyatomic Molecules*; Van Nostrand: Princeton, 1968; p 178.
33. Spirko, V.; Kraemer, W. P. *J. Mol. Spec.* **1992**, *153*, 285.
34. Kondratiev, V. N. *Natl. Stand. Ref. Data Ser.* (US), **1972**, NSRDS-COM-72-10014.
35. (a) Fukui, K. *Acc. Chem. Res.* **1981**, *14*, 363. (b) Page, M.; Melver, J. W., Jr. *J. Chem. Phys.* **1988**, *88*, 922.
36. Lee, Y. T.; McDonald, J. D.; LeBreton, P. R.; Herschbach, D. R. *J. Chem. Phys.* **1968**, *49*, 2447.
37. Mullins, C. B.; Rettner, C. T.; Auerbach, D. J. *J. Chem. Phys.* **1991**, *95*, 8649.
38. Herzberg, G. *Spectra of Diatomic Molecules*; Van Nostrand: Princeton, 1967; p 101.
39. Valero, R.; Kroes, G.-J. *J. Phys. Chem. A* **2004**, *108*, 8672.
40. Johnston, H. S.; Goldfinger, P. *J. Chem. Phys.* **1962**, *37*, 700.
41. Bell, T. N.; Perkins, K. A.; Perkins, P. G. *J. Phys. Chem.* **1977**, *81*, 2610.
42. Robinson, P. J.; Holbrook, K. A. *Unimolecular Reactions*; Wiley: New York, 1972; p 103.
43. Polanyi, J. C. *Acc. Chem. Res.* **1972**, *5*, 161.
44. Levine, R. D.; Bernstein, R. B. *Molecular Reaction Dynamics and Chemical Reactivity*; Oxford Univ. Press: New York, 1987; pp 148-156.